Research Square

Preprints are preliminary reports that have not undergone peer review.
They should not be considered conclusive, used to inform clinical practice,
or referenced by the media as validated information.

Investigating tattoo particles in the porcine model using X-ray phase-contrast tomography

Simon Zandarco

simon.zandarco@tum.de

Technical University of Munich

Dominik John

Technical University of Munich

Sami Wirtensohn

Technical University of Munich

Amelie Pfeiffer

Technical University of Munich

Felix Beckmann

Helmholtz-Zentrum Hereon

Julian Moosmann

Helmholtz-Zentrum Hereon

Jörg Hammel

Helmholtz-Zentrum Hereon

Imke Greving

Helmholtz-Zentrum Hereon

Silja Flenner

Helmholtz-Zentrum Hereon

Patrick Ilg

Technical University of Munich

Ines Schreiver

Federal Institute for Risk Assessment

Crysta De Cuyper

AZ Sint-Jan

Isabelle Rooms

AZ Sint-Jan

Franz Pfeiffer

Technical University of Munich

Julia Herzen

Technical University of Munich

Madleen Busse

Technical University of Munich

Article

Keywords:

Posted Date: October 28th, 2026

DOI: https://doi.org/10.21203/rs.3.rs-10878872/v1

License: This work is licensed under a Creative Commons Attribution 4.0 International License.
Read Full License

Additional Declarations: No competing interests reported.

Investigating tattoo particles in the porcine model using X-ray phase-contrast tomography

Simon Zandarco[1,2,*], Dominik John[2,3,4], Sami Wirtensohn[2,3,4,5], Katharina A. Pfeiffer[2,3], Felix Beckmann[4], Julian Moosmann[4], Jörg U. Hammel[4], Imke Greving[4], Silja Flenner[4], Patrick Ilg[1,2], Ines Schreiver[6], Christa de Cuyper[7], Isabelle Rooms[7], Franz Pfeiffer[1,2,8,9], Julia Herzen[2,3], and Madleen Busse[1,2,10]

[1]Chair of Biomedical Physics, Department of Physics, TUM School of Natural Sciences, Technical University of Munich, 85748 Garching, Germany
[2]Munich Institute of Biomedical Engineering, Technical University of Munich, 85748 Garching, Germany
[3]Research Group Biomedical Imaging Physics, Department of Physics, TUM School of Natural Sciences, Technical University of Munich, 85748 Garching, Germany
[4]Institute of Materials Physics, Helmholtz-Zentrum hereon, 21502 Geesthacht, Germany
[5]Centre for X-Ray and Nano Science CXNS, Deutsches Elektronen-Synchrotron (DESY), Notkestraße 85, 22607 Hamburg, Germany
[6]Department of Chemical and Product Safety, Dermatotoxicology Study Centre, German Federal Institute for Risk Assessment (BfR), Berlin, Germany
[7]Department of Dermatology, AZ Sint-Jan, Ruddershove 10, 8000 Bruges, Belgium
[8]Department of Diagnostic and Interventional Radiology, TUM School of Medicine, Klinikum rechts der Isar, Technical University of Munich, 81675 München, Germany
[9]TUM Institute for Advanced Study, Technical University of Munich, 85748 Garching, Germany
[10]Department of Biological Safety, German Federal Institute for Risk Assessment (BfR), Berlin, Germany
[*]simon.zandarco@tum.de

ABSTRACT

In industrialized countries, an estimated 10 to 20 % of the population carries at least one tattoo, making the dermal deposition and systemic migration of tattoo pigments a relevant public-health concern. Their biokinetics remain poorly understood, partly due to a lack of suitable imaging methods. Here, we present a multi-scale, multimodal imaging approach that combines synchrotron-radiation single-grid phase-contrast X-ray micro-computed tomography (micro-CT), synchrotron-radiation Zernike phase-contrast X-ray nano-CT (nano-CT), and transmission electron microscopy (TEM) to investigate tattooed skin in a 28-day porcine model and in a human biopsy with an allergic reaction to an unknown red pigment. Micro-CT resolved the 3D distribution of pigment agglomerates within segmented skin layers and tracked the immune response at days 7, 14, and 28, revealing swelling at day 7 that subsided by day 28. Volume quantification recovered only 6.4 % of the expected TiO_2 content, revealing a key limitation of micro-CT. Nano-CT resolved the internal architecture of these agglomerates at higher resolution, showing individual TiO_2 particles remain separated by soft tissue rather than merging. TEM complemented both modalities by visualizing single TiO_2, copper phthalocyanine (CuPh), and weakly absorbing red pigment particles undetectable by CT alone. Together, these modalities span length scales from whole biopsies to single nanoparticles, offering a framework for evaluating tattoo ink safety in dermatology, toxicology, and regulation.

Introduction

In industrialized countries, an estimated 10 to 20 % of the population carries at least one tattoo, leading to widespread exposure to inks that can be absorbed and distributed in the body[1,2]. Beyond body art, such as permanent make-up, tattoos also have medical uses, such as nipple–areola reconstruction after mastectomy[3,4]. Due to concerns about hazardous ink components, the EU introduced unified chemical regulations in 2020, while oversight in other countries remains inconsistent[5–7]. These regulatory efforts respond to a range of documented health effects in tattooed individuals. Adverse reactions to tattoos can occur locally within the tattooed area or, in some cases, manifest systemically[8]. Allergic reactions in red tattoos linked to organic azo pigments are a particular challenge, and metal abrasion from needles may also release sensitizing metals[9]. Despite recent reviews, the biokinetics of tattoo inks remain poorly understood[10]. Previous studies addressed the metabolism of tattoo pigments in rat and human microsomal systems[11], and showed a partial disappearance of pigment from mouse skin within

six weeks[12] as well as its distribution to other organs such as the liver[13]. A recent study has extended this work to a porcine model[14] using a blue tattoo ink (Periwinkle, Eternal Ink EUROPE GmbH, Germany) that mainly consists of TiO_2 and copper phthalocyanine blue (CuPh; CI 74160)[15]. Porcine skin closely resembles human skin, but its properties vary across anatomical sites; the study therefore focused on the inner thigh, which most closely matches human skin in both thickness and texture. The findings show that tattoo ink migrates from the skin to the lymph nodes within 28 days, with no detectable distribution to other organs[14]. In the present study, we further investigate the skin of these pigs. In addition, two human biopsies are examined, one with an allergic reaction to a similar blue tattoo ink (also containing TiO_2 and CuPh) and one to an unknown organic red pigment. For this purpose, we employ a multi-scale imaging approach combining micro- and nano-CT with transmission electron microscopy (TEM). These techniques were assessed both for the insights they provide into the biokinetics of tattoo particles within the skin and for their suitability in future tattoo pigment studies.

Results

Micro-CT

A slice of a biopsy obtained from healthy, tattooed pig skin on day 28 and acquired using the micro-CT setup is shown in Fig. 1(a). To assess the agglomeration of tattoo particles within the skin, the individual skin layers, epidermis, dermis, and hypodermis, were segmented using *Dragonfly 3D World 2025* (Comet Technologies Canada Inc.). Tattoo particles were segmented using a threshold of $395\,\mathrm{nm}^{-3}$ and above and are highlighted in light green. Fig. 1(c) shows a line profile through a tattoo particle and highlights in green the segmented region. The adipose tissue clearly separates the hypodermis from the dermis. During dehydration with ethanol and clearing with xylol, lipid content is extracted[16,17], leaving voids in the tissue that are subsequently filled with paraffin during embedding. The paraffin-filled regions within the hypodermis are indicated by the yellow arrow. In addition, two blood vessels are marked by turquoise arrows. Individual tattoo particles are too small to be detected directly, as their sizes (TiO_2: $389.3 \pm 16.8\,\mathrm{nm}$; CuPh: $61.3 \pm 2.3\,\mathrm{nm}$) are smaller than the effective pixel size ($p_{\mathrm{eff}} = 2.554\,\mu\mathrm{m}$). However, as previously reported[18], these particles form agglomerates within the skin that are detectable by micro-CT imaging. These agglomerates are clearly observed below the epidermis in the upper dermis. CT imaging allows quantification of their depth below the skin surface. The mean depth was determined to be $163 \pm 90\,\mu\mathrm{m}$, and the corresponding depth distribution is shown in Fig. 1(b). This depth should be regarded as approximation, as the embedding process caused substantial deformation of the sample. To evaluate whether CT imaging can quantify tattoo particle volume, we determined the total segmented volume as $0.093\,\mathrm{mm}^3$. Subsequently, the segmented volume was used to render a three-dimensional volume in Suppl. Fig. S3.

The morphological changes of the skin over time at 7, 14, and 28 days after tattooing are shown in Fig. 2(a), (b), and (c), respectively. In addition, regions of interest (ROIs) at the different time points are shown in Fig. 2(d–i). By day 7, the tattoo particles have accumulated beneath the epidermis. Furthermore, a skin swelling reaction is present where no tattoo particles are present. By day 14, the swelling of the skin had reduced, diminishing the distance between them and the epidermis. Furthermore, an immune response is evident, with several particle clusters being encapsulated and subsequently expelled from the skin. At day 28, neither immune reactions nor swelling are detectable in the skin. The tattoo particles also accumulated in a smaller region within the skin. In Fig. 4(a) and (d), micro-CT slices of the porcine skin tattooed with the blue ink, already shown above, and of the human biopsy with the organic red pigment are depicted, respectively. The micro-CT of the human skin biopsy from the allergic reaction to the unknown red pigment reveals significant morphological differences that extend beyond the usual variance between human and porcine skin. The tattooed human skin shows a granulomatous dermatitis, which is common for red tattoos, and pseudolymphomatous inflammation. The epidermis on the bottom is visibly thickened and partially ruptured on the left. The dermis is divided into a lower- and a higher-electrondensity layer, suggesting increased collagen density as part of the immune response. The small, darker nodules beneath the epidermis, indicated by the black and yellow arrows in Suppl. Fig. S2, likely represent accumulations of immune cells.

Nano-CT

The samples were further investigated at higher resolution using the nano-CT to examine the behavior of individual TiO_2 particles within the tissue. Fig. 3(a) and (b) show slices through two different ROIs of the skin sample harvested at day 7 after tattooing. A ROI containing tattoo particles is shown in Fig. 3(c). In Fig. 3(a), the particles are more dispersed and show only minor agglomerates, whereas in Fig. 3(b) they exhibit more pronounced clustering. Despite this local accumulation, most particles remain separated by soft tissue and do not merge into a single larger particle.

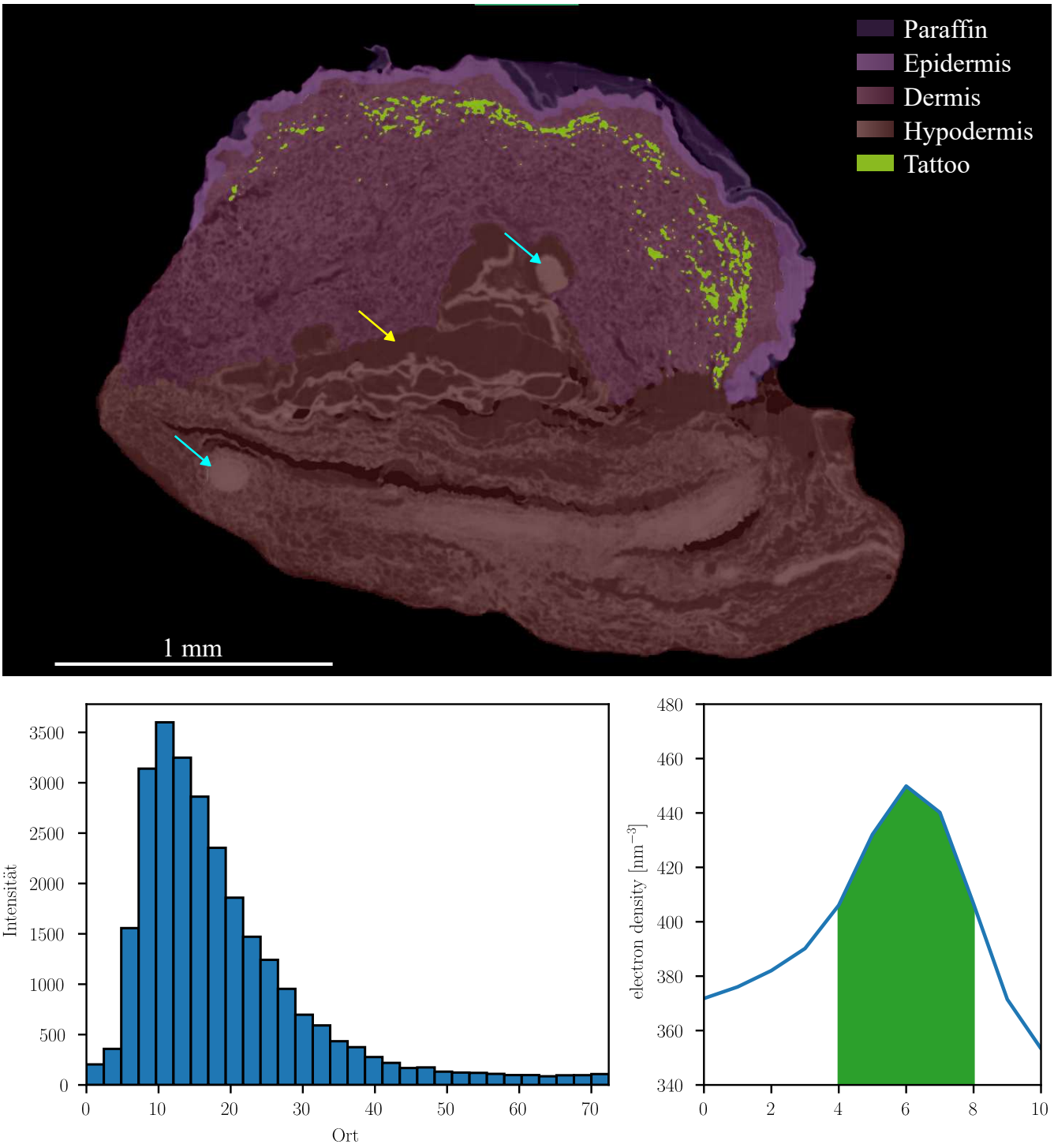

Figure 1. Segmented tomogram of electron density of tattooed porcine skin at day 28. In (a) the epidermis, the dermis, and the hypodermis are segmented, as well as the paraffin in which it is embedded. The tattoo particles, highlighted in bright green, agglomerate beneath the epidermis in the upper region of the dermis. The depth distribution is plotted in (b). (c) plots the signal through a tattoo particle agglomerate and shows the signal identified as tattoo particles.

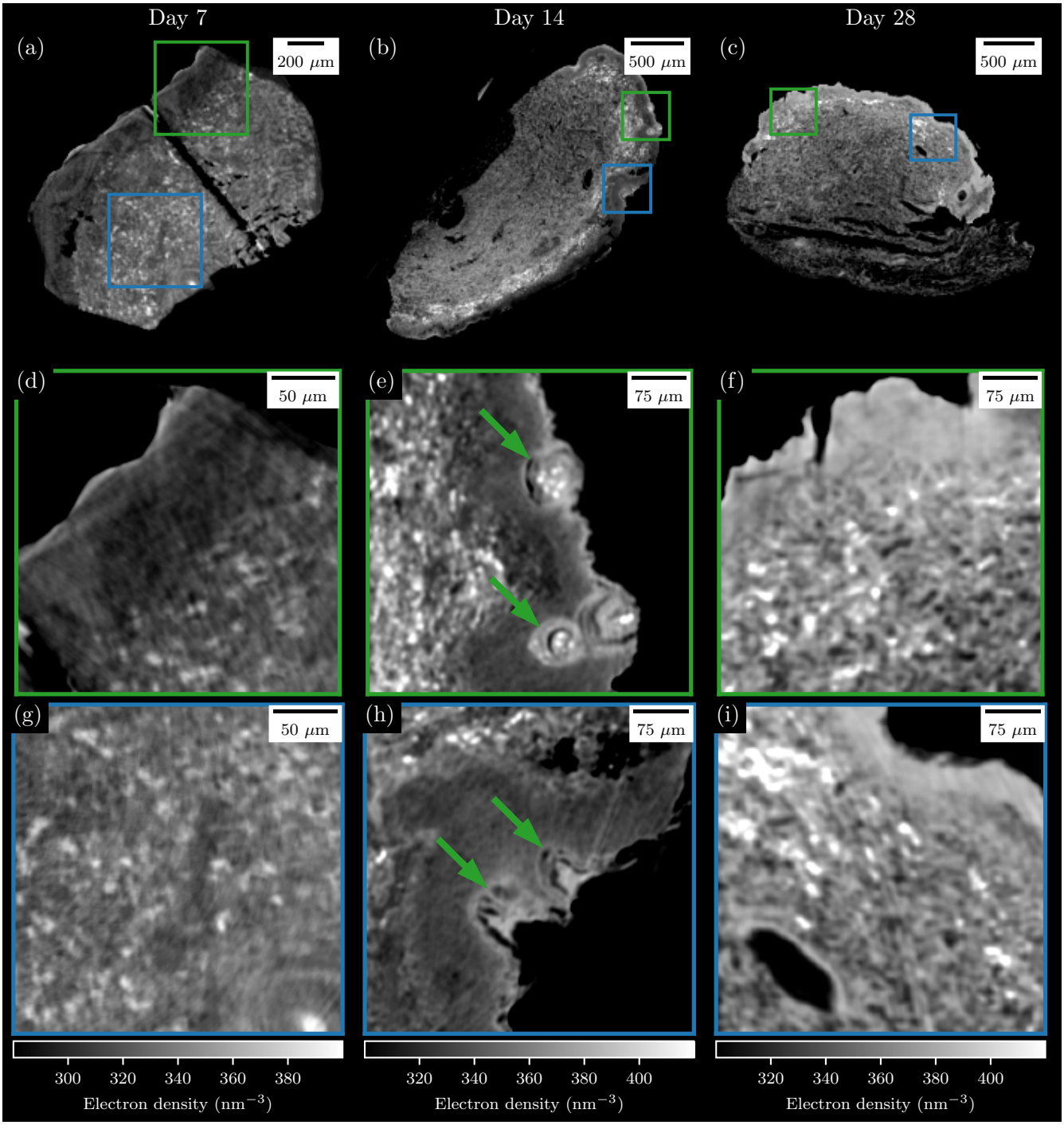

Figure 2. The tomograms of electron density of the tattooed porcine skin harvested at day 7, day 14, and day 28 are shown in (a), (b), and (c), respectively. The ROIs in (a), (b), and (c) are depicted in (d) & (g), (e) & (h), and in (f) & (i), respectively.

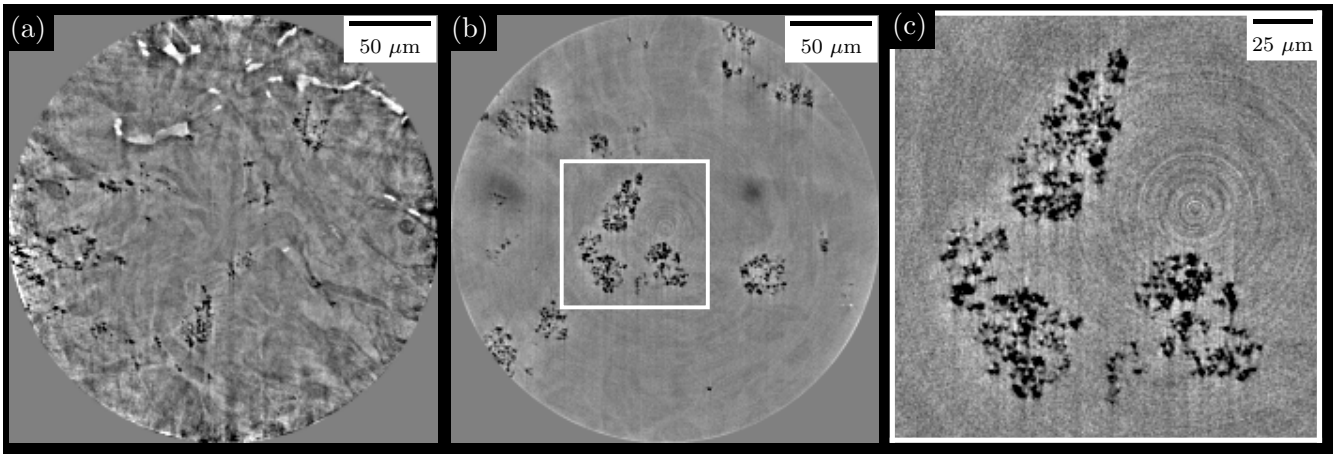

Figure 3. Tomograms acquired at the nano-CT setup. (a) and (b) show a slice through two different ROIs from the skin sample at day 7 tattooed with the blue ink. The TiO_2 particles are visible in black. (c) shows a ROI within (b) where single tattoo particles are visible. The images are all windowed the same for maximum visibility.

TEM

Lastly, the sample was investigated using TEM. Using the micro-CT images in Fig. 4 (a, d), a ROI was selected for TEM imaging, for further investigation of the tattoo ink deposited in the skin. As depicted in Fig. 4 (b, c, e, f) all three different color molecules, TiO_2, CuPh and the organic red color, are detectable, as pointed out by the blue, white, and red arrows, respectively. Because the different pigments exhibit distinct structures and sizes, they are distinguishable.

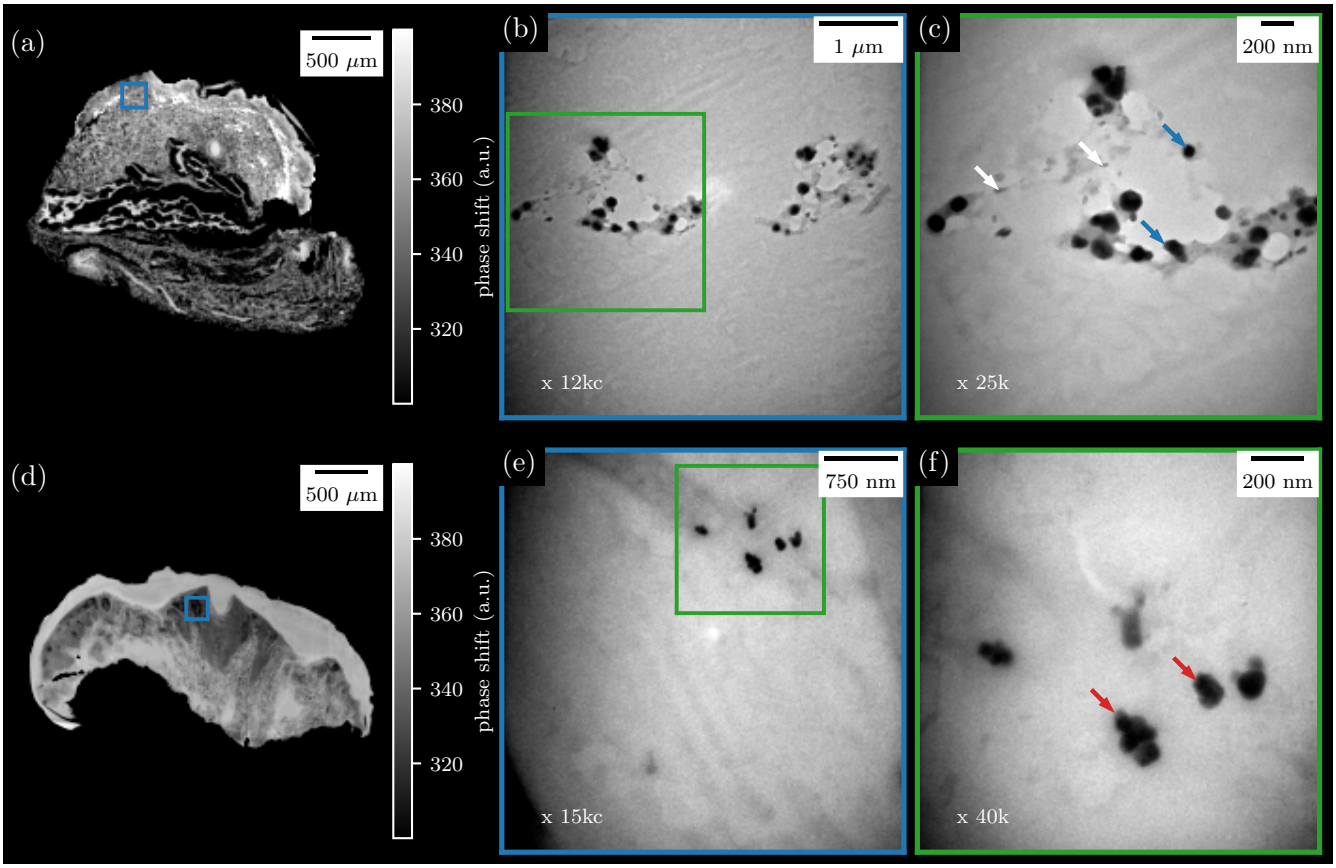

Figure 4. Images acquired using the micro-CT setup, (a) and (d), and TEM imaging, (b, c, e, f). The porcine skin tattooed with the blue ink is shown in (a-c), while the human skin biopsy with the organic red pigment is depicted in (d-f). Examples of the different pigments are indicated by blue (TiO_2), white (CuPh), and red (organic red pigment) arrows.

Discussion

The aim of this work was to further investigate tattooed skin using several imaging setups and to evaluate their feasibility for the analysis of tattoo inks.

Initially, the samples tattooed with the blue tattoo ink were examined at the micro-CT setup. As shown in Fig. 1, the segmentation of tattoo particles was possible, although they are smaller than the effective pixel size of the setup, due to their tendency to form agglomerates. In addition, the different skin layers could be clearly distinguished and segmented, allowing investigation of the spatial distribution of tattoo particles within the tissue. The majority of the particles were found beneath the epidermis, primarily within the upper dermal layer, as further shown in Suppl. Fig. S3. However, the exact depth distribution remains difficult to determine because the sample undergoes deformation during the embedding process.

To account for this deformation, the shrinkage of the surface area of the embedded skin sample was quantified using Lindblad's weighted local configurations algorithm[19]. The calculated surface area of the embedded sample was 12.8 mm^2, compared with 28.3 mm^2 for the untreated sample, corresponding to the area of the 6 mm punch. This corresponds to a shrinkage of 54.7 % in two dimensions and 32.7 % in one dimension. Assuming similar shrinkage behavior for the dermis and hypodermis as for the epidermis, a corrected mean particle depth of $242 \pm 134\,\mu mm$ was estimated. However, this assumption may not be fully valid. While no studies on porcine skin shrinkage during paraffin embedding are available, investigations on canine[20–22] and feline skin[23] report a wide range of shrinkage in one surface dimension, ranging from 18.0 % to 37.7 %. The shrinkage observed in this study is therefore consistent with published values. Interestingly, studies on cat and dog cadavers reported an unintuitive effect: although samples shrank in length and width, the tissue depth increased by up to 75.8 %[20,23]. Assuming a maximal depth expansion of 75.8 %, the corrected mean particle depth would be $92.7 \pm 51.2\,\mu m$. Nevertheless, no indication of the unintuitive depth expansion reported in canine and feline studies was observed for the epidermis, suggesting that $220 \pm 122\,\mu m$ is likely closer to the true value.

CT imaging was further evaluated as a method to quantify the volume of tattoo particles. Cambiaso et al.[14] reported a titanium content of $130 \pm 40\,g/m^2$, which corresponds to 1.45 mm^3 of pure TiO_2 in the sample taken by the 6 mm punch. However, only a volume of 0.093 mm^3 was detected, corresponding to just 6.4 % of the expected content. Thus, quantitative volume determination of tattoo particles proved unfeasible. Several factors may contribute to this discrepancy. First, not all TiO_2 particles form agglomerates. Particles that are homogeneously distributed within the dermis remain below the detection limit, as their size is smaller than the effective pixel size. These particles contribute only to a slight increase in background intensity that cannot be reliably distinguished. Second, the segmentation threshold was conservatively selected to minimize noise originating from dermal tissue. As illustrated in Fig. 1(c), a line profile across a tattoo particle shows that only part of the particle width can be confidently assigned due to the absence of a well-defined edge. This effect can lead to a substantial underestimation of particle volume, particularly in three-dimensional reconstructions.

In contrast, imaging tattooed skin at several time points after tattooing (see Fig. 2) demonstrated strong potential for investigating the tissue response to tattooing, including allergic reactions, which are frequently associated with red tattoo pigments. Distinct morphological changes were observed at the three investigated time points, suggesting that a more detailed temporal study with shorter intervals would be highly informative. In the present specimen, pronounced skin swelling was observed at day 7. The tattoo particles accumulate beneath the swelling and are thus detectable, yet remain widely distributed throughout the skin. By day 14, the immune response persisted, but the swelling had decreased. Additionally, another immune response became apparent: the skin attempts to encapsulate the tattoo particles and expel them from the tissue. The shedding of tattoo particles by the skin is evident in the skin rendering in Suppl. Fig. S4. While some particles are removed in this process, the majority remain within the skin. By day 28, the immune response appears to have subsided, and the tattoo particles remain stationary beneath the epidermis. Notably also the region over which the tattoo particles are distributed was reduced in comparison to day 7.

While these macroscopic tissue responses could be characterized using the micro-CT setup, the behavior of individual tattoo particles could not be resolved at the micro-CT scale. For this reason, measurements at the nano-CT setup were of particular interest. At this scale, individual TiO_2 particles could be directly imaged and analyzed. As shown in Fig. 3(a), particles are initially dispersed within the tissue, although agglomeration has already begun. Figures 3(b) and (c) present zoomed-in views of one agglomerate, like the ones that were previously segmented in the micro-CT dataset. Contrary to the expectation that particles would merge into a uniform structure, individual particles remain separated by soft tissue. In addition, isolated particles and small clusters are visible. These observations confirm that micro-CT alone cannot recover the full tattoo particle volume. Individual particles simply remain below its resolution limit.

Furthermore, we investigated the human skin tattooed with the organic red pigment (Fig. 4 (d)). Organic red pigments are known to cause allergic reactions[9]. Although the red pigment itself provides insufficient contrast to be imaged directly with micro-CT, the morphological changes it induces in the skin can still be investigated. The reaction was pronounced but differed markedly from that caused by the blue ink: whereas the blue pigment, both in the porcine skin at day 7 and in the human skin (Suppl. Fig. S1), produced swelling of the subepidermal tissue, the red pigment induced strong swelling of the epidermal

tissue together with an accumulation of immune cells, as shown in Suppl. Fig. S2. The micro-CT data of both human and porcine skin can be used to identify and select small regions of interest for subsequent TEM analysis. In the blue tattooed skin, both TiO_2 and CuPh particles can be directly visualized. Notably, TEM is the only imaging modality in this work capable of visualizing CuPh particles. This confirms their presence in the tattooed skin alongside TiO_2. Furthermore, TEM enables the detection of the organic red pigment in the red-tattooed skin. Although its particles are comparable in size to the TiO_2, they appear to cluster far less: while Fig. 4 (c) shows roughly 20 to 30 TiO_2 particles, Fig. 4 (f) depicts only about five. This suggests two complementary explanations for why micro-CT cannot image the red pigment: the electron-density difference to the surrounding tissue is too small, and too few particles accumulate to be visualized. The clustering behavior of different tattoo inks should therefore be the subject of further investigation.

The combination of the three imaging modalities provides comprehensive insight into the morphology and distribution of tattoo particles within the skin. Micro-CT imaging enables the visualization of larger particle agglomerates and therefore provides information about the spatial localization of tattoo pigments. In addition, it reveals structural changes associated with the skin's immune response. Nano-CT imaging complements these findings by providing higher spatial resolution, allowing a more detailed investigation of the particle agglomerates. At this resolution scale, the internal structure of the TiO_2 agglomerates becomes visible, including soft tissue components located within the aggregates. Finally, TEM enables the detection of even smaller particles, such as CuPh, as well as weakly absorbing materials like the organic red pigment. In future work, scanning electron microscopy (SEM) combined with energy-dispersive X-ray spectroscopy (EDX) could further support the chemical characterization of individual particles.

Overall, the multimodal imaging approach presented in this work demonstrates strong potential for advancing tattoo ink research. By combining complementary imaging techniques across multiple length scales, we achieve a more detailed understanding of the distribution, morphology, and tissue interactions of tattoo pigments. This can improve the evaluation and selection of newly approved tattoo inks — and ultimately increase safety for the growing tattooed population. Additionally, as tattoo particles are a form of nanoparticulate materials, the multimodal imaging approach will advance nanoparticle research at the tissue particle interface.

Material and Methods

Experimental Setups

Three different setups were used in this work to enable measurement at different length scales and using different modalities. In the following, the main parameters of the micro-CT, nano-CT and transmission electron microscopy (TEM) setups are briefly described.

Micro-CT

The micro-CT experiments were conducted at the High Energy Materials Science Beamline P07, which is operated by Helmholtz-Zentrum Hereon at PETRA III, DESY in Hamburg, Germany[24–26]. A sketch of the experimental setup is depicted in Fig. 5 (a). The beam originates from a 4 m long in-vacuum undulator and is filtered to the desired energy using a bent Laue double-crystal monochromator. For all experiments in this work, an energy of $E = 37\,\mathrm{keV}$ was used to balance sufficient transmission through the metal-containing tattoo particles with the stronger phase-contrast achievable at lower energies. The X-ray beam first passes a modulator, which is a Talbot array illuminator with a period of 10 µm[27]. Its design height corresponds to imparting a $2\pi/3$ phase shift to parts of an X-ray wavefront with an energy of 40 keV, which was the closest available specification to the energy used in the experiment. Next, the beam passes through the sample, which is located on a rotation stage at a distance $l = 175\,\mathrm{mm}$ from the modulator. Lastly, the X-rays reach the scintillator, placed a further distance $d = 700\,\mathrm{mm}$ downstream. It is connected to a CMOS-based camera with an array of 6720×4764 pixels, each with a pixel size of 6.9 µm. Together with the 5.1-fold magnifying optics, the calibrated effective pixel size after 2-fold binning was 2.554 µm. The projection data were acquired by continuously rotating the sample by 180° while capturing 3001 projections with an exposure time of 50 ms each. After each tomographic scan, the modulator was moved into its next lateral position, and the scanning procedure was repeated for a total of 16 modulator positions. Further information is given in the Suppl. Sec "Micro-CT Data processing".

Nano-CT

The nano-CT experiments were conducted at the Nanotomography endstation of the P05 beamline operated by the Helmholtz-Zentrum Hereon at PETRA III, DESY in Hamburg, Germany, as depicted in Fig. 5 (b). At the P05 beamline, the X-rays are produced by an U29 Undulator with a length of 2 m. It creates a $36.0\,\mu\mathrm{m} \times 6.1\,\mu\mathrm{m}$ large source size with a divergence of $28.0\,\mu\mathrm{rad} \times 4.0\,\mu\mathrm{rad}$[28]. A Si-111 double crystal monochromator tunes the energy to 11 keV. The images are acquired with a Hamamatsu C12849-101U detector, which has a pixel size of 6.5 µm and a chip size of 2048×2048 pixels. A direct 1:1 coupled 10 µm thick scintillator is utilized for visual light conversion[29]. For the measurements, a Zernike phase-contrast Transmission

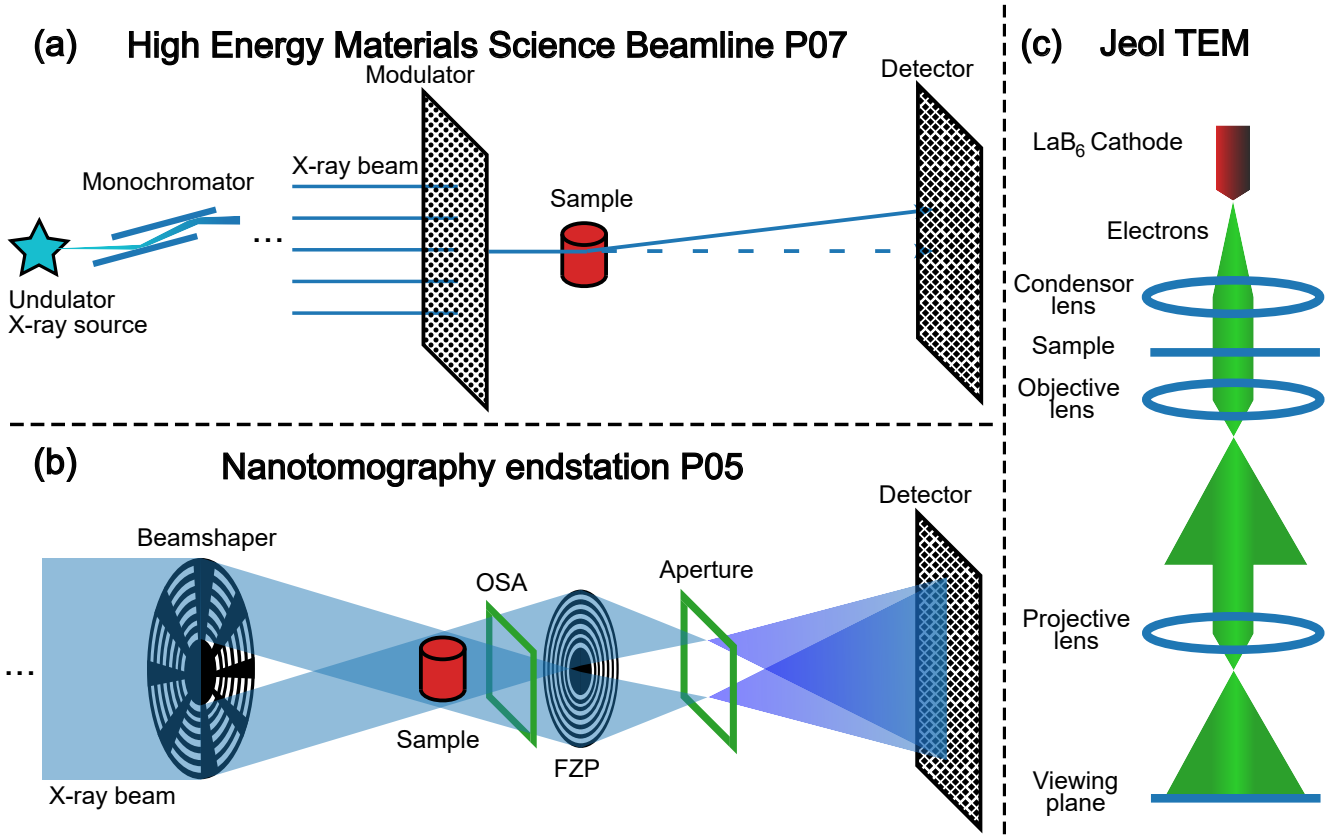

Figure 5. Schematics of the three imaging setups used in this work. (a) Single-grid phase-contrast micro-CT setup at beamline P07 (PETRA III, DESY), where the monochromatized X-ray beam passes through a Talbot array illuminator (modulator) before impinging on the sample, and the beam deflection induced by the sample is recorded at the detector. (b) Zernike phase-contrast nano-CT setup at the P05 beamline (PETRA III, DESY), using a beam-shaping condenser, an Order Sorting Aperture(OSA) and a Fresnel zone plate (FZP) as the objective lens placed behind the sample. (c) Transmission electron microscopy (TEM) setup (JEOL JEM 1400 Plus, BfR).

X-ray Microscope (TXM) was set up. It uses a beam-shaping condenser as a first optic with 100 µm × 100 µm large fields and a Fresnel Zone Plate (FZP) as an objective lens, which is placed behind the sample[30]. The FZP is made out of gold with a diameter of 300 µm and an outermost zone width of 50 nm, resulting in an unbinned effective pixel size of 46.41 nm. To create the enhanced phase-contrast, a $\frac{\pi}{2}$-shifting phase ring is placed in the back focal plane of the FZP. Due to the refraction within the sample, the path of the interacting X-rays is changed. Hence, only a part of the beam passes through the phase ring and receives the additional phase shift. The non-shifted and shifted parts of the beam interfere at the detector, creating a contrast boost[29]. The data is acquired with a continuous sample rotation over a range of 180° and 3112 projections, each exposed for 250 ms. Afterward, they are reconstructed with TomoPy[31].

Transmission Electron Microscopy (TEM)

The TEM images were acquired using a Jeol TEM, the JEM 1400 Plus, outlined in Fig. 5 (c). The TEM was operated at 120 kV and 64 µA. Individual cells were first surveyed at magnifications of 12 000× to 15 000×, which suffices to spot intracellular nanomaterials. Cells containing such material were then imaged at 25 000× to 40 000× magnification. The images were acquired with an Olympus camera using the software ITEM (Olympus, Version ITEM-E-23082007). Further image analysis, such as the measurement of dimensions (length, width, and diameter), was carried out using Image J (Version 1.53a).

Samples

In this work, a total of seven porcine skin samples, of which four are shown in this paper, and two human skin biopsies were investigated. While the porcine samples were obtained from a dedicated study, the human biopsies stem from clinical routine.

Tattoo Inks

For the porcine study, the ink with the highest titanium content was selected from ten different tattoo inks (*Periwinkle*, Eternal Ink EU ROPE GmbH, Germany). The two main components of the tattoo ink were TiO_2 and CuPh blue (CI 74160)[15]. The titanium content is 211.49± 3.79 g/kg and the copper content is 5.68± 0.01 g/kg. The TiO_2 particles have a mean diameter of 389.3± 16.8 nm, an attenuation coefficient of $\mu_{TiO_2} = 7.54\,cm^{-1}$ at an energy of 36.86 keV and an electron density of $1221\,nm^{-3}$ at a density of $4.26\,g/cm^3$[32]. The CuPh particles with a diameter of 61.3± 2.3 nm only have an attenuation coefficient of $\mu_{CuPh} = 1.42\,cm^{-1}$ at 36.86 keV and an electron density of $496\,nm^{-3}$ at a density of $1.62\,g/cm^3$[33]. A blue ink with the same main components (TiO_2 and CuPh) was also present in one of the human tattoos sampled at the hospital, which allowed us to study these pigments in human skin as well. In addition, a biopsy containing an unknown red pigment was taken. This sample was of particular interest, as red tattoo inks are more prone to allergic reactions than inks of other colors.

Human

The two human tissue samples investigated in this work were obtained during standard therapeutic procedures performed as part of routine clinical care at AZ Sint-Jan Brugge AV, Bruges, Belgium, and not as part of a study or experiment. The Ethics Committee (Commissie voor Ethiek) of AZ Sint-Jan Brugge AV (chair: Dr. Barbara Brouwers) reviewed this case report (internal EC no. 3920; Belgian registration number B0492026000013) and approved its publication on 9 October 2026, under the conditions that professional confidentiality is respected, written informed consent was obtained, and the anonymity of the patients is guaranteed. Written informed consent was obtained from both patients for the use of the collected material for scientific purposes and publication. All methods were carried out in accordance with the relevant guidelines and regulations, including the Declaration of Helsinki. The first tattoo was located on the right upper arm and contained an unknown organic red pigment. The patient exhibited two independent allergic reactions, a pseudolymphomatous and a granulomatous reaction, in 2013 and 2022. On both occasions, the tattoo was treated by shaving, and in 2022, shades of brown were visible at the tattoo site. The second sample is from a tattoo extending from the left thigh to the ankle joint, which showed an allergic reaction to the blue tattoo ink containing titanium dioxide (TiO_2) and CuPh.During the first weeks of the patient's second pregnancy, the most recently applied blue tattoos showed skin reactions with itchiness and plaques, while older sites tattooed with the same blue pigment reacted more weakly. As the affected areas became infected, the patient underwent antibiotic treatment. Further information about the patients is subject to data-protection regulations.

Animal

All porcine skin samples were collected as part of Janos Cambiaso-Daniel *et al.*'s study of tattoo pigment biokinetics in vivo in a 28-day porcine model[14]. The study began in April 2022 and lasted four weeks, during which the animals were anesthetized four times. Tattooing was performed on day 1, followed by punch biopsies on days 7, 14, and 28. Skin biopsies were obtained using 6 mm punch biopsies and were collected under general anesthesia, sutured with a single stitch, and covered with a medical dressing. The samples collected after 7, 14, and 28 days are displayed using the micro-CT setup. From the sample taken at day 7, additional punch biopsies were taken for investigation at the nano-CT setup. Further information is given in the Suppl. Sec "Sample preparation". All animal procedures were approved by the Austrian Federal Ministry of Education, Science and Research (BMBWF; application no. 2020-0.193.102) and conducted in accordance with Directive 2010/63/EU. This study is

reported in accordance with the ARRIVE guidelines. Four female pigs (8 weeks old; 19.6± 2.7 kg) were acclimatized for 10 days before the study and housed in pairs with free access to food and water. All procedures were performed by veterinarians and/or qualified personnel. After euthanasia on day 28, the regional lymph nodes and selected internal organs were collected. As no significant amount of tattoo particles has been found in any of the internal organs, they have been excluded from this study. Detailed procedures of anesthesia, euthanasia, tattooing, and organ removal are provided by Cambiaso *et al.*[14] and are available in Suppl. Sec. Animal Procedures.

Acknowledgments

The authors acknowledge Helmholtz-Zentrum Hereon (Geesthacht, Germany) and DESY (Hamburg, Germany) for providing the experimental facilities. This research was carried out at PETRA III. Beamtime was allocated for proposal I-20240214. This research was supported in part through the Maxwell computational resources operated at Deutsches Elektronen-Synchrotron DESY, Hamburg, Germany. Measurements were taken during the following beamtimes: 11019133, 11020977, 11019748, 11022861, 11023681. The authors gratefully acknowledge financial support by the following grants: The ERC Consolidator Grant (Julia Herzen, TUM, DEPICT, PE3, 101125761) and the EIC Pathfinder (Julia Herzen, TUM, 1MICRON, 101186826). Furthermore, this study was financially supported by a BfR internal grant (1322-808). D. J. acknowledges a doctoral scholarship from the Friedrich Naumann Foundation for Freedom, funded by the Bundesministerium für Forschung, Technologie und Raumfahrt (BMFTR). The authors thank Dr. Janos Cambiaso-Daniel for providing the pig skin samples.

Author contributions statement

M.B., F.P., and J.H. conceived the experiments. I.S., C.d.C., and I.R. provided the samples, and M.B. chemically prepared them. D.J., J.M., F.B., and J.U.H. conducted the micro-CT experiments; S.W., I.G., and S.F. conducted the nano-CT experiments; and M.B. performed the TEM measurements. P.I. rendered the volumes. M.B. and S.Z. coordinated the project. K.A.P. and S.Z. analyzed the results, and S.Z. wrote the main manuscript text and prepared the figures. All authors reviewed the manuscript.

Statement of Ethics

The animal study protocol was reviewed and approved by the Austrian Federal Ministry of Education, Science and Research, approval number BMBWF 2020-0.193.102. Publication of the human case report was approved by the Ethics Committee (Commissie voor Ethiek) of AZ Sint-Jan Brugge AV (internal EC no. 3920; B0492026000013).

Conflict of Interest Statement

There is no financial interest in any of the products, devices, or drugs discussed in the manuscript. All the authors declare no conflict of interest.

Data Availability Statement

The data that support the findings of this study are not publicly available but are available from the corresponding author upon reasonable request.

References

1. Kluger, N. Epidemiology of tattoos in industrialized countries. *Curr Probl Dermatol* **48**, 6–20 (2015).
2. Roberts, A. E., Koch, J. R., Armstrong, M. L. & Owen, D. C. Correlates of tattoos and reference groups. *Psychol. Reports* **99**, 933–934 (2006).
3. Ghafari, G., Newcomer, J., Rigali, S. & Liszewski, W. Permanent makeup: A review of its technique, regulation, and complications. *J. Am. Acad. Dermatol.* **91**, 690–698 (2024).
4. Vassileva, S. & Hristakieva, E. Medical applications of tattooing. *Clin. Dermatol.* **25**, 367–374 (2007).
5. Wang, X. *et al.* Analytical survey of tattoo inks—a chemical and legal perspective with focus on sensitizing substances. *Contact Dermat.* **85**, 340–353 (2021).
6. European Commission. Commission regulation (EU) 2020/2081 of 14 December 2020 amending annex XVII to regulation (EC) No 1907/2006 of the European Parliament and of the Council concerning the registration, evaluation, authorisation and restriction of chemicals (REACH) as regards substances in tattoo inks or permanent make-up. Official Journal of the European Union L 423, 6–17 (2020).

7. Laumann, S. Regulation of tattoo ink production and the tattoo business in the us. *Tattooed Ski. Heal.* **48**, 248–252 (2015).
8. Serup, J., Sepehri, M. & Hutton Carlsen, K. Classification of tattoo complications in a hospital material of 493 adverse events. *Dermatology* **232**, 668–678 (2017).
9. Schreiver, I. *et al.* Distribution of nickel and chromium containing particles from tattoo needle wear in humans and its possible impact on allergic reactions. *Part. Fibre Toxicol.* **16**, 33 (2019).
10. Serup, J. From technique of tattooing to biokinetics and toxicology of injected tattoo ink particles. *Diagn. Ther. Tattoo Complicat. With Atlas Illus. Cases* **52**, 1–17 (2017).
11. Cui, Y., Churchwell, M. I., Couch, L. H., Doerge, D. R. & Howard, P. C. Metabolism of pigment yellow 74 by rat and human microsomal proteins. *Drug metabolism disposition* **33**, 1459–1465 (2005).
12. Bäumler, W. Absorption, distribution, metabolism and excretion of tattoo colorants and ingredients in mouse and man: the known and the unknown. *Curr Probl Dermatol* **48**, 176–84 (2015).
13. Sepehri, M., Sejersen, T., Qvortrup, K., Lerche, C. M. & Serup, J. Tattoo pigments are observed in the kupffer cells of the liver indicating blood-borne distribution of tattoo ink. *Dermatology* **233**, 86–93 (2017).
14. Cambiaso-Daniel, J. *et al.* Tattoo pigment biokinetics in vivo in a 28-day porcine model: elements undergo fast distribution to lymph nodes and reach steady state after 7 days. *Dermatology* **240**, 304–311 (2024).
15. Serup, J. *et al.* Identification of pigments related to allergic tattoo reactions in 104 human skin biopsies. *Contact Dermat.* **82**, 73–82 (2020).
16. Lerch, M. L. *et al.* Monitoring dehydration and clearing in tissue processing for high-quality clinical pathology. *Biopreservation biobanking* **17**, 303–311 (2019).
17. Carriel, V., Campos, F., Aneiros-Fernández, J. & Kiernan, J. A. Tissue fixation and processing for the histological identification of lipids. In *Histochemistry of Single Molecules: Methods and Protocols*, 197–206 (Springer, 2017).
18. Itin, P. & Jemec, G. *Diagnosis and therapy of tattoo complications: with atlas of illustrative cases* (Karger Medical and Scientific Publishers, 2017).
19. Lindblad, J. & Nyström, I. Surface area estimation of digitized 3d objects using local computations. In *International Conference on Discrete Geometry for Computer Imagery*, 267–278 (Springer, 2002).
20. Reagan, J. K., Selmic, L. E., Garrett, L. D. & Singh, K. Evaluation of the effects of anatomic location, histologic processing, and sample size on shrinkage of skin samples obtained from canine cadavers. *Am. journal veterinary research* **77**, 1036–1044 (2016).
21. Reimer, S. B., Séguin, B., DeCock, H. E., Walsh, P. J. & Kass, P. H. Evaluation of the effect of routine histologic processing on the size of skin samples obtained from dogs. *Am. journal veterinary research* **66**, 500–505 (2005).
22. Upchurch, D. A., Malenfant, R.-C., Wignall, J. R., Ogden, D. M. & Saile, K. Effects of sample site and size, skin tension lines, surgeon, and formalin fixation on shrinkage of skin samples excised from canine cadavers. *Am. journal veterinary research* **75**, 1004–1009 (2014).
23. Jeyakumar, S. *et al.* Effect of histologic processing on dimensions of skin samples obtained from cat cadavers. *Am. J. Vet. Res.* **76**, 939–945 (2015).
24. Schell, N. *et al.* The high energy materials science beamline (HEMS) at PETRA III. In *Materials Science Forum*, vol. 772, 57–61 (Trans Tech Publ, 2014).
25. John, D. *et al.* Recent developments in quantitative phase-contrast microtomography using Talbot array illuminators. *Dev. X-ray Tomogr. XV* **13152**, 109–116 (2024).
26. John, D. *et al.* Quantitative stain mapping in X-ray virtual histology. *Adv. Sci.* e19783 (2026).
27. Gustschin, A. *et al.* High-resolution and sensitivity bi-directional x-ray phase contrast imaging using 2D Talbot array illuminators. *Optica* **8**, 1588–1595 (2021).
28. Wirtensohn, S. *et al.* Directional dark field for nanoscale full-field transmission x-ray microscopy. *Light. Sci. & Appl.* **15**, 223, DOI: 10.1038/s41377-026-02263-z (2026).
29. Wirtensohn, S. *et al.* Nanoscale dark-field imaging in full-field transmission x-ray microscopy. *Optica* **11**, 852–859, DOI: 10.1364/OPTICA.524812 (2024).
30. Jefimovs, K., Vila-Comamala, J., Stampanoni, M., Kaulich, B. & David, C. Beam-shaping condenser lenses for full-field transmission x-ray microscopy. *J. Synchrotron Radiat.* **15**, 106–108, DOI: 10.1107/S0909049507047711 (2008).

31. Gürsoy, D., De Carlo, F., Xiao, X. & Jacobsen, C. TomoPy: a framework for the analysis of synchrotron tomographic data. *J. Synchrotron Radiat.* **21**, 1188–1193, DOI: 10.1107/S1600577514013939 (2014).

32. Shi, H., Magaye, R., Castranova, V. & Zhao, J. Titanium dioxide nanoparticles: a review of current toxicological data. *Part. fibre toxicology* **10**, 15 (2013).

33. PubChem. Copper phthalocyanine. https://pubchem.ncbi.nlm.nih.gov/compound/Copper-phthalocyanine.

Supplementary Files

This is a list of supplementary files associated with this preprint. Click to download.

- renderingd28video.mp4
- renderingd14video.mp4
- SupplementarymaterialInvestigatingtattooparticlesintheporcinemodelusingXrayphasecontrasttomography.pdf